Enhancement of the Spin Hall Angle by Interdiffusion of Atoms in $Co_2FeAl_{0.5}Si_{0.5}$/*n*-Ge Heterostructures

Shingo Kaneta-Takada,[1,*] Michihiro Yamada,[2] Shoichi Sato,[1] Shoma Arai,[1] Le Duc Anh,[1,3] Kohei Hamaya,[2] and Shinobu Ohya[1,3,4,†]

[1] *Department of Electrical Engineering and Information Systems, The University of Tokyo, Bunkyo, Tokyo 113-8656, Japan*

[2] *Center for Spintronics Research Network, Graduate School of Engineering Science, Osaka University, 1-3 Machikaneyama, Toyonaka 560-8531, Japan*

[3] *Institute of Engineering Innovation, The University of Tokyo, Bunkyo, Tokyo 113-8656, Japan*

[4] *Center for Spintronics Research Network (CSRN), The University of Tokyo, Bunkyo, Tokyo 113-8656, Japan*

(Received 27 January 2020; revised 6 April 2020; accepted 16 July 2020; published 31 August 2020)

Realizing efficient spin-charge conversion is an important issue in spin-based electronics, especially for the development of low-power-consumption magnetization switching. A spin-charge conversion is generally induced in a nonmagnetic (NM) layer by the inverse spin Hall effect in the bulk or by the inverse Rashba-Edelstein effect at surfaces or interfaces. In the bulk, the spin-charge conversion efficiency is called the spin Hall angle, θ_{SHE}, and it is limited by the spin-orbit interaction of the bulk layer. Thus, artificially enhancing θ_{SHE} to greater than its intrinsic value is difficult. Here, using spin-pumping measurements on a well-controlled interface between a ferromagnetic (FM) $Co_2FeAl_{0.5}Si_{0.5}$ (CFAS) layer and a NM *n*-type Ge layer, we demonstrate that θ_{SHE} can be strongly enhanced by annealing the sample and the resulting interdiffusion of atoms within only about 3.7 nm around the CFAS/*n*-Ge interface. Because of this annealing process, θ_{SHE} is increased from 0.0058–0.0079 to 0.015–0.019, which is much larger than the intrinsic value of θ_{SHE} reported for Ge (0.00096–0.002) and is comparable to θ_{SHE} values reported for Pt. This enhancement is attributed to strong scattering of the spin current in the intermixed layer formed at the interface by annealing. Our results indicate that θ_{SHE} is strongly influenced by the atomic structure of the FM/NM interface, which suggests an efficient method to control spin-charge conversion by precise control of the FM/NM interface.

DOI: 10.1103/PhysRevApplied.14.024096

I. INTRODUCTION

In the research field of spintronics, which is expected to generate next-generation devices that overcome the limitations of complementary metal-oxide-semiconductor technology, the realization of a highly efficient spin-charge-current conversion is extremely important, especially for the development of functional devices, such as spin-orbit torque magnetic random access memory [1–4]. The spin current can be generated by various methods, such as electrical spin injection [5,6], thermal excitation [7,8], spin pumping [9], and optical spin orientation [10]. Among them, spin pumping is believed to be a very efficient way to inject a pure spin current from a ferromagnetic (FM) layer into a nonmagnetic (NM) layer using ferromagnetic resonance (FMR) in FM/NM bilayer systems [11,12]. The injected spin current is converted into the charge current by the inverse spin Hall effect (ISHE) in the NM layer, where its efficiency, the so-called spin Hall angle, θ_{SHE}, is limited by the spin-orbit interaction (SOI) of this layer. Thus, artificially controlling θ_{SHE} is generally difficult when the same material system is used. Here, using spin pumping, we demonstrate that θ_{SHE} can be enhanced to more than the intrinsic value of the NM layer due to a slight interdiffusion of atoms at the FM/NM interface. Our result indicates that θ_{SHE} is strongly influenced by the atomic structure at the FM/NM interface, which expands the possibility of efficiently controlling spin-charge conversion with a low power consumption by controlling atomic ordering at FM/NM interfaces. This work is an experiment that compares the results obtained by the four-terminal electrical spin-injection and spin-pumping measurements, which will help to improve our understanding about details of the spin-injection process.

*skaneta@cryst.t.u-tokyo.ac.jp
†ohya@cryst.t.u-tokyo.ac.jp

II. SAMPLE PREPARATION AND EXPERIMENTAL SETUP

For experiments, we use a sample composed of $Co_2FeAl_{0.5}Si_{0.5}$ (CFAS) (25 nm)/P-doped *n*-Ge (doping concentration: $6–7 \times 10^{18}$ cm^{-3}) (140 nm)/undoped Ge(111) buffer layer (100 nm) grown on a Si (111) substrate by molecular beam epitaxy (MBE) [Fig. 1(a)]. CFAS is chosen as the ferromagnetic spin injector because we can make an atomically sharp interface between CFAS and Ge due to their good lattice matching (the mismatch is ∼0.4%) [13]. The CFAS layer in our heterostructure has both L_{21}-order and B_2-order phases, and thus, it is not halfmetallic. We note that the lattice strain in Ge due to the lattice mismatch between Ge and Si is fully relaxed in the undoped Ge buffer layer. We also prepare a reference sample comprising a single layer of CFAS (25 nm) that is directly grown on an undoped Ge(111) substrate by MBE, in which a generated spin current is negligible. We hereafter refer to this sample as a reference sample. This reference sample is needed because we estimate the spin current density using the difference in the peak-to-peak FMR line widths of the CFAS layer with and without spin-current injection and absorption. In our sample grown on Si, two pairs of a P δ-doped Ge layer (3 and 4 nm) and an ultrathin Si layer (0.3 nm) are inserted at the interface between the CFAS and *n*-Ge layers. These ultrathin Si layers can suppress the segregation of P atoms to the surface during MBE growth, enabling us to have precise control of the P concentration in the P δ-doped Ge layers [14]. This δ-doping technique can decrease the Schottky barrier width and tunneling resistance between CFAS and *n*-Ge [Fig. 1(b)], playing a crucial role in efficient spin injection and detection in electrical measurements [14,15]. We anneal part of the sample at a low temperature of 300 °C for 10 min in N_2 gas at ambient pressure, which induces interdiffusion of the atoms in the vicinity of the CFAS/*n*-Ge interface, but this process does not affect the transport properties of *n*-Ge [16]. As shown in the scanning transmission electron microscopy (STEM) images [Figs. 2(a) and 2(c)], a highly crystalline CFAS/*n*-Ge interface is produced in both

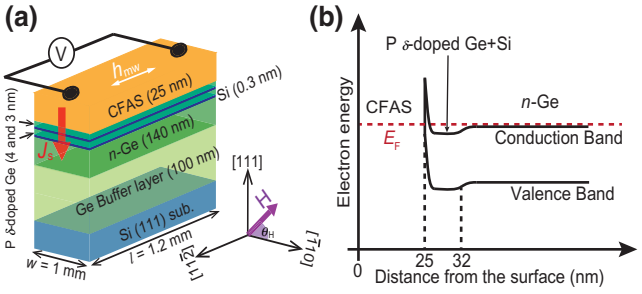

FIG. 1. (a) Schematic structure of the CFAS/*n*-Ge sample. All layers are epitaxially grown by MBE. (b) Band alignment close to the CFAS/*n*-Ge interface.

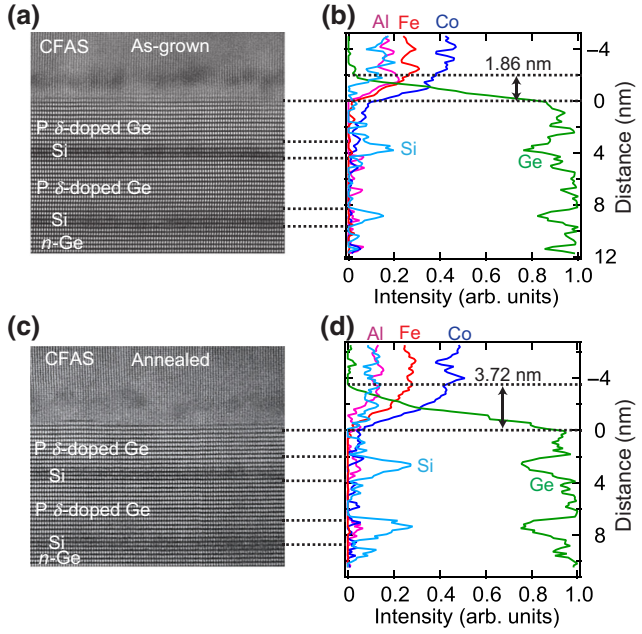

FIG. 2. STEM lattice images in the vicinity of the interface between CFAS and *n*-Ge in (a) as-grown and (c) annealed samples. EELS spectral intensity in the vicinity of the CFAS/*n*-Ge interface in (b) as-grown and (d) annealed samples. Region between dashed lines corresponds to the intermixed region between CFAS and *n*-Ge layers. Thickness of the intermixed region in the annealed sample is clearly larger than that in the as-grown sample.

the as-grown and annealed samples. However, when we carefully look at the interface using electron energy-loss spectroscopy (EELS) [Figs. 2(b) and 2(d)], the annealed sample has an interdiffused area (∼3.7 nm) that is twice that of the as-grown sample (∼1.9 nm) at the CFAS/*n*-Ge interface (see the area between the broken lines). In previous electrical measurements [16] that used this annealing process for a CFAS/P δ-doped Ge interface, the spin-injection and -detection efficiency, P_S, *decreased* due to this interdiffusion. Meanwhile, as shown below, our spin-pumping experiments reveal that θ_{SHE} is *enhanced* by annealing.

III. RESULTS

A. Electrical transport and electrical spin-injection measurements

The resistivity, ρ_{Ge}, of *n*-Ge is measured using a four-terminal method for a lateral spin-valve device made from our CFAS/*n*-Ge sample [see the green line in Fig. 3(a)]. Details of the fabrication process of this device are described in Refs. [15,17,18]. To obtain the resistivity, ρ_{CFAS}, of CFAS, we prepare a sample composed of a CFAS layer (25 nm) directly grown on a MgO substrate by MBE. Because the MgO substrate is highly resistive, we can obtain the resistivity only of CFAS by measuring

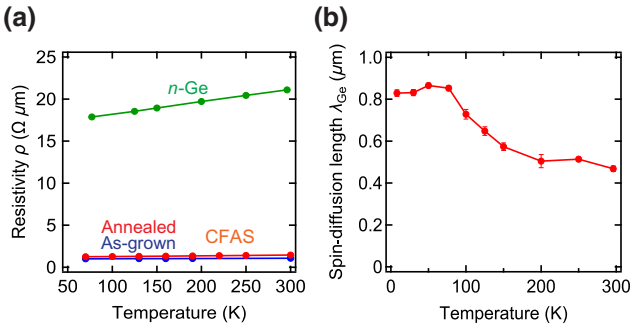

FIG. 3. (a) Temperature dependence of the resistivities ρ_{Ge} (of *n*-Ge) and ρ_{CFAS} (of CFAS) of as-grown and annealed samples. (b) Temperature dependence of the spin-diffusion length, λ_{Ge}, in *n*-Ge with a carrier density of 6–7 $\times 10^{18}$ cm^{-3}.

the resistance of this sample [see the red and blue lines in Fig. 3(a)]. ρ_{Ge} and ρ_{CFAS} monotonically decrease with decreasing temperature. Electrical spin-injection measurements are carried out on a lateral spin-valve device made from our CFAS/*n*-Ge sample. From the obtained spin signals, the spin-diffusion length λ_{Ge} of Ge is estimated as shown in Fig. 3(b). The detailed method of the estimation of λ_{Ge} is described in Refs. [15,17,18].

B. Spin-pumping measurements

For the as-grown and annealed CFAS/*n*-Ge samples, we carry out spin-pumping measurements using a transverse electric TE_{011} cavity in an electron spin-resonance system with a microwave frequency of 9.1 GHz and with various microwave powers (MPs), ranging from 10 to 100 mW. For measurements, as shown in Fig. 1(a), a static magnetic field, H, is applied along the $[\bar{1}10]$ direction of the Ge layer in the film plane (i.e., $\theta_H = 0°$ or 180°), which corresponds to the easy magnetization axis of CFAS. Here, θ_H is defined as the out-of-plane angle of H with respect to the in-plane $[\bar{1}10]$ axis. The microwave magnetic field, h_{mw}, is applied along the $[11\bar{2}]$ direction in the film plane. As shown in the H dependence of the electromotive force (EMF), $V(H)$, for various MPs at 300 K, with $\theta_H = 0$ and 180° [Figs. 4(a) and 4(b)], the EMF is enhanced at the FMR field, H_{FMR} (=85 mT), and the EMF monotonically increases with increasing MP, which are typical results of spin-pumping experiments. The most noticeable point is that the magnitude of the EMF in the annealed sample is significantly larger than that in the as-grown sample.

To extract the signal of the ISHE, we decompose the EMF into a symmetric component, V_{sym}, which includes the signal of the ISHE, and an asymmetric component,

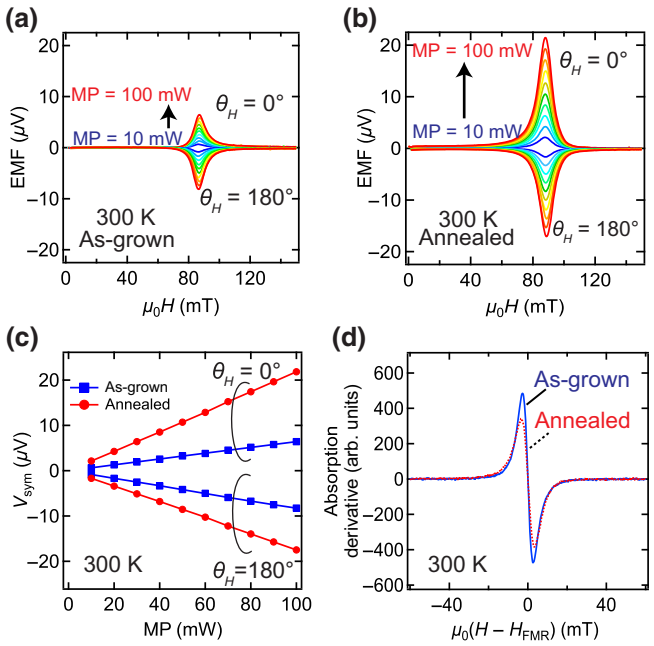

FIG. 4. Magnetic field, H, dependencies of the EMF at 300 K measured for (a) as-grown and (b) annealed samples with various MP values, ranging from 10 to 100 mW. In the electron-spin-resonance system, a microwave magnetic field, h_{mw}, is applied along the $[11\bar{2}]$ direction of the Ge layer. (c) MP dependences of the symmetric component V_{sym} in the as-grown and annealed samples. (d) Magnetic field, H, dependences of the microwave-absorption derivative for as-grown and annealed samples at 300 K with MP = 50 mW.

V_{asym}, using the following equation:

$$V(H) = V_{sym}\frac{\Delta H^2}{(H - H_{FMR})^2 + \Delta H^2} + V_{asym}\frac{-2\Delta H(H - H_{FMR})}{(H - H_{FMR})^2 + \Delta H^2}, \quad (1)$$

where ΔH is the half width at half maximum of the FMR line width. As shown in Fig. 4(c), we see a linear relation between the MP and V_{sym}. To extract the signal of the ISHE, the sign of which should be reversed with a reversal in the H direction, and to eliminate the contribution of the Seebeck effect, we derive $V_{sym,ave}$, which is defined as $(V_{sym,0°} - V_{sym,180°})/2$, where $V_{sym,0°}$ and $V_{sym,180°}$ are the V_{sym} values for $\theta_H = 0°$ and 180°, respectively.

Next, we estimate the spin current density, $j_S^{CFAS/n\text{-Ge}}$, from the mixing conductance, $g_r^{\uparrow\downarrow}$. Here, $g_r^{\uparrow\downarrow}$ is obtained from the difference in the FMR peak-to-peak line widths between the CFAS/*n*-Ge sample ($\Delta H_{pp,CFAS/n\text{-Ge}}$), which is shown in Fig. 4(d), and the reference sample ($\Delta H_{pp,CFAS}$), where the spin-current injection is negligible,

as follows:

$$g_r^{\uparrow\downarrow} = \frac{4\pi M_S d_{\mathrm{CFAS}}}{g\mu_{\mathrm{B}}}(\alpha_{\mathrm{CFAS}/n\text{-Ge}} - \alpha_{\mathrm{CFAS}}), \quad (2)$$

where M_S, d_{CFAS}, g, μ_{B}, $\alpha_i = \sqrt{3}\gamma\Delta H_{\mathrm{pp},i}/(2\omega)$ ($i =$ CFAS/n-Ge and CFAS), γ, and ω are the saturation magnetization of CFAS, the thickness of the CFAS layer, the g factor [19], the Bohr magneton, the damping constant of the CFAS/n-Ge sample and reference sample, the gyromagnetic ratio, and the angular frequency, respectively. For the estimation of $g_r^{\uparrow\downarrow}$ for the annealed sample, we use a 29.5% smaller value of α_{CFAS} than that of the reference sample, following the experimental results in Ref. [13]. [In Ref. [13], Kuerbanjiang *et al.* estimated the damping constants using the frequency dependence of the resonance-field line width in the as-grown CFAS layer grown on a Ge(111) substrate and those annealed at 350 and 450 °C. The damping constant is decreased by 32.1% and 48.2% by annealing at 350 and 450 °C, respectively. Supposing that the damping constant linearly decreases as the annealing temperature increases from 25 to 450 °C, the damping constant of the sample annealed at 300 °C is estimated to be 29.5% smaller than that of the as-grown sample.] We note that M_S at 300 K decreases from 921 to 709 emu/cm^3 by annealing at 300 °C. This behavior is also shown in Ref. [16]. The decrease in saturation magnetization is confirmed at all temperatures. We also note that the influence of the extrinsic line width component of CFAS [13] is cancelled out in Eq. (2).

We derive $j_S^{\mathrm{CFAS}/n\text{-Ge}}$ by using

$$j_S^{\mathrm{CFAS}/n\text{-Ge}} = \frac{g_r^{\uparrow\downarrow}\gamma^2 h_{\mathrm{mw}}^2\hbar\left[4\pi M_S\gamma + \sqrt{(4\pi M_S)^2\gamma^2 + 4\omega^2}\right]}{8\pi\alpha_{\mathrm{CFAS}/n\text{-Ge}}{}^2[(4\pi M_S)^2\gamma^2 + 4\omega^2]}, \quad (3)$$

where $\hbar$ is the Dirac constant. The estimated value of $j_S^{\mathrm{CFAS}/n\text{-Ge}}$ is 5.70×10^{-11} J/m^2 for the as-grown sample and 6.25×10^{-11} J/m^2 for the annealed sample. The parameters used for the derivation of the spin current are shown in Table I. The estimated value of $j_S^{\mathrm{CFAS}/n\text{-Ge}}$ is not largely different between the as-grown and annealed samples. Finally, we estimate θ_{SHE} using the following equation:

$$V_{\mathrm{sym,ave}} = \frac{l\theta_{\mathrm{SHE}}\lambda_{\mathrm{Ge}}\tanh(d_{\mathrm{Ge}}/2\lambda_{\mathrm{Ge}})}{\sigma_{\mathrm{Ge}}d_{\mathrm{Ge}} + \sigma_{\mathrm{CFAS}}d_{\mathrm{CFAS}}} \times \left(\frac{2e}{\hbar}\right) j_S^{\mathrm{CFAS}/n\text{-Ge}}, \quad (4)$$

TABLE I. Physical values used for the estimation of the spin current density at 300 K.

	As-grown	Annealed
$\alpha_{\mathrm{CFAS}/n\text{-Ge}}$	0.0149	0.0174
α_{CFAS}	0.00931	0.00776
M_S (T)	1.16	0.891

where σ_{Ge}, σ_{CFAS}, d_{Ge}, and d_{CFAS} are the conductivities and thicknesses of the n-Ge and CFAS layers, respectively; l is the length of the sample [see Fig. 1(a)]; and e is the elementary charge.

The obtained temperature dependences of the EMF, current density, and estimated θ_{SHE} in the as-grown and annealed samples are shown in Figs. 5(a), 5(b), and Figs. 6(a), 6(b). The estimated θ_{SHE} is 0.0058–0.0079 for the as-grown sample and 0.015–0.019 for the annealed sample. Both values are nearly independent of temperature, which means that the contributions of the anomalous and planar Hall effects are negligibly small because these are proportional to ρ^n [see Fig. 3(a)], where n is 1–2 [20]. The θ_{SHE} values for both samples are much higher than those previously reported for Ge ($\theta_{\mathrm{SHE}} \sim 0.00096$–$0.002$ [21–23]). In the case of the as-grown sample, the large θ_{SHE} values can be partly attributed to the high-quality all-epitaxial single-crystal layers and to nearly no contribution from the random magnetic stray fields due to the sharp FM/NM interface, as shown in the STEM images [Figs. 2(a) and 2(c)]. As discussed below, the effect of the slight interdiffusion of atoms at the FM/NM interface (∼1.9 nm) may also be another cause of this large θ_{SHE}. The most important finding herein is that θ_{SHE} for the annealed sample is much larger than that for the as-grown sample at all temperatures, which means that θ_{SHE} is very sensitive to the atomic structure of the FM/NM interface. Surprisingly, the θ_{SHE} values obtained for the annealed sample are comparable to values reported for Pt ($\theta_{\mathrm{SHE}} = 0.012$–$0.12$ [24–26]).

C. Confirmation of the negligibly small ISHE signal in the reference sample

We measure the temperature dependence of the EMF induced by the ISHE in the reference sample with a microwave power of 50 mW and estimate the generated current density [Fig. 6(a)]. We subtract the current density obtained for the reference sample from those obtained for the as-grown and annealed samples and estimated the spin

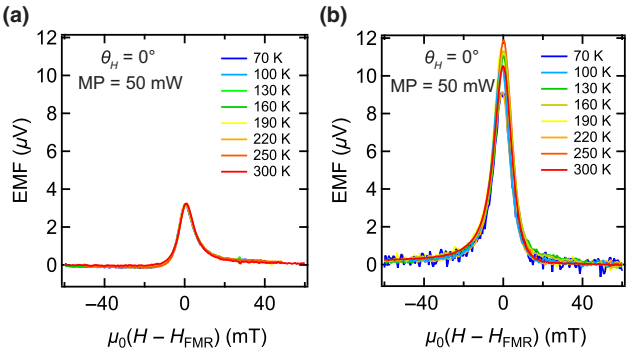

FIG. 5. Magnetic field, H, dependence of the EMF obtained with MP = 50 mW for (a) as-grown and (b) annealed samples at various temperatures, ranging from 70 to 300 K. H is applied along the [$\bar{1}$10] direction.

Hall angle, θ_{SHE} [Fig. 6(b)], by using

$$V_{\mathrm{sym,ave}}\frac{\sigma_{\mathrm{Ge}}d_{\mathrm{Ge}}+\sigma_{\mathrm{CFAS}}d_{\mathrm{CFAS}}}{l\lambda_{\mathrm{Ge}}\tanh\left(\frac{d_{\mathrm{Ge}}}{2\lambda_{\mathrm{Ge}}}\right)} - V^{\mathrm{ref}}_{\mathrm{sym,ave}}\frac{\sigma^{\mathrm{ref}}_{\mathrm{Ge}}d^{\mathrm{ref}}_{\mathrm{Ge}}+\sigma_{\mathrm{CFAS}}d_{\mathrm{CFAS}}}{l\lambda^{\mathrm{ref}}_{\mathrm{Ge}}\tanh\left(\frac{d^{\mathrm{ref}}_{\mathrm{Ge}}}{2\lambda^{\mathrm{ref}}_{\mathrm{Ge}}}\right)} = \theta_{\mathrm{SHE}}\left(\frac{2e}{\hbar}\right)j_S^{\mathrm{CFAS}/n\text{-Ge}},$$

where $V^{\mathrm{ref}}_{\mathrm{sym,ave}}$ is $(V^{\mathrm{ref}}_{\mathrm{sym},0^\circ} - V^{\mathrm{ref}}_{\mathrm{sym},180^\circ})/2$, where $V^{\mathrm{ref}}_{\mathrm{sym},0^\circ}$ and $V^{\mathrm{ref}}_{\mathrm{sym},180^\circ}$ are the V_{sym} values obtained for the reference sample for $\theta_H = 0°$ and 180°, respectively; $\lambda^{\mathrm{ref}}_{\mathrm{Ge}}$ is the spin-diffusion length of n-Ge when the doping concentration is very low (1×10^{16} cm^{-3}) [27]. We confirm that there is not a large difference between the θ_{SHE} values before and after subtraction of the signal obtained for the reference sample [Fig. 6(b)].

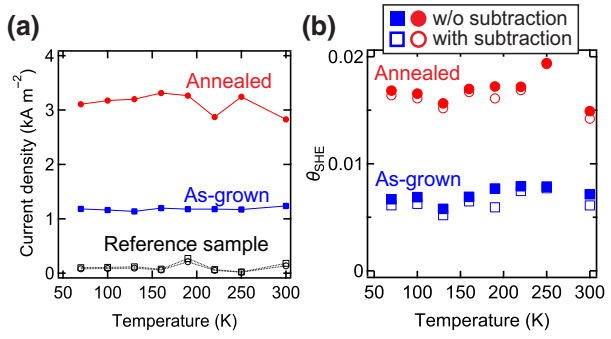

FIG. 6. (a) Temperature dependences of the density of the current generated by the ISHE in the as-grown sample, annealed sample, and reference sample with MP = 50 mW. (b) Temperature dependence of θ_{SHE} of as-grown and annealed samples before and after subtracting the current density of the reference sample.

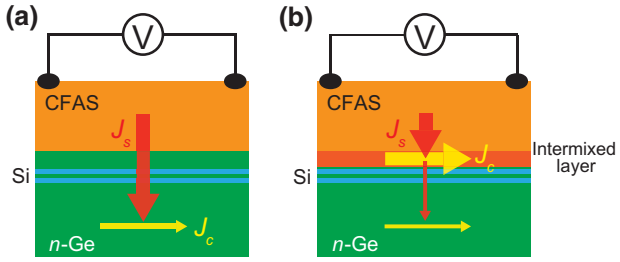

FIG. 7. Difference in spin-charge-conversion processes between (a) as-grown and (b) annealed samples. In (a), spin current, J_s, is efficiently injected into n-Ge and converted into charge current, J_c, in n-Ge. In (b), J_s is not efficiently injected into n-Ge due to strong scattering in the intermixed layer and is converted into J_c in the intermixed layer.

IV. DISCUSSION

Here, using the θ_{SHE} values obtained in our study and the P_S values obtained in the electrical measurements in Ref. [16], we discuss the physical nature of the spin-charge conversion process in our samples. The previous study in Ref. [16] reported that the P_S drastically decreased upon annealing. Meanwhile, our spin-pumping experiment shows the opposite behavior; after annealing, θ_{SHE} is increased from 0.0058–0.0079 to 0.015–0.019. These results can be explained using Fig. 7. In the as-grown sample, the spin current, J_s, is efficiently injected into n-Ge due to the elevated P_S [Fig. 7(a)], and then the J_s is converted into the charge current, J_c, in the n-Ge layer through the ISHE. In the case of the annealed sample, however, J_s is not efficiently injected into n-Ge, reflecting the decreased P_S [Fig. 7(b)]. The intermixing layer strongly disturbs J_s due to the strong SOI, which converts J_s into J_c very efficiently. Here, the injected J_s is *not* completely converted into J_c in the intermixing layer, but a small amount of J_s flows into n-Ge and is converted into J_c in n-Ge [Fig. 7(b)]. This scenario suggests that the intermixed layer has potential as an efficient spin-charge converter.

Although the inverse Rashba-Edelstein effect (IREE) is reported for the Fe/Ge(111) interface [28], this is not likely to be the origin of our EMF signals. The IREE length, λ_{IEE}, is proportional to the mean free path, λ, of electrons [29], while θ_{SHE} is inversely proportional to the spin-diffusion length, λ_s. If the IREE mainly worked in our samples, the EMF of the as-grown sample would be larger than that of the annealed one because λ and λ_s near the CFAS/n-Ge interface should be larger due to smaller interdiffusion in the as-grown sample than that of the annealed sample. However, our results are opposite. Therefore, we can conclude that the ISHE works in the intermixing layer.

The abovementioned results also indicate that identifying the origin of θ_{SHE} obtained in spin-pumping experiments is very difficult, even in bilayer structures. Because interdiffusion of atoms within only about 3.7 nm strongly influences the θ_{SHE} value, we need a careful analysis of the atomic structure and the distribution of atoms in FM/NM samples used in spin-pumping experiments.

V. SUMMARY

We investigate how the interdiffusion of atoms induced by annealing influences θ_{SHE} in a CFAS/*n*-Ge heterostructure using spin pumping. After annealing, θ_{SHE} is strongly enhanced from 0.0058–0.0079 to 0.015–0.019. These values are larger than those previously reported for Ge. Furthermore, θ_{SHE} of the annealed sample is comparable to values reported for Pt. This result is opposite to the behavior of P_S obtained by previous transport measurements; P_S in that case decreases after annealing. The increased P_S and decreased θ_{SHE} in the as-grown sample indicate that the spin current is efficiently injected into *n*-Ge and spin-charge conversion occurs in *n*-Ge. Meanwhile, decreased P_S and increased θ_{SHE} in the annealed sample indicate that the spin current is converted into the charge current due to the large SOI of the intermixing layer formed at the interface. Our result indicates that θ_{SHE} is strongly influenced by the atomic structure of the FM/NM interface. These results help to explain detailed processes of spin-charge conversion and spin injection in FM/NM bilayer structures, which provide a method of producing highly efficient spin-charge conversion by controlling the interdiffusion of atoms.

ACKNOWLEDGMENTS

This work is partly supported by Grants-in-Aid for Scientific Research (Grants No. 18H03860 and No. 19H05616), CREST of JST (Grant No. JPMJCR1777), and the Spintronics Research Network of Japan (Spin-RNJ).

[1] J. C. Slonczewski, Current-driven excitation of magnetic multilayers, J. Magn. Magn. Mater. **159**, L1 (1996).
[2] L. Berger, Emission of spin waves by a magnetic multilayer traversed by a current, Phys. Rev. B **54**, 9353 (1996).
[3] I. M. Miron, K. Garello, G. Gaudin, P. J. Zermatten, M. V. Costache, S. Auffret, S. Bandiera, B. Rodmacq, A. Schuhl, and P. Gambardella, Perpendicular switching of a single ferromagnetic layer induced by in-plane current injection, Nature **476**, 189 (2011).
[4] L. Liu, C.-F. Pai, Y. Li, H. W. Tseng, D. C. Ralph, and R. A. Buhrman, Spin-Torque switching with the giant spin hall effect of tantalum, Science **336**, 555 (2012).
[5] F. J. Jedema, H. B. Heersche, A. T. Filip, J. J. A. Baselmans, and B. J. van Wees, Electrical detection of spin precession in a metallic mesoscopic spin valve, Nature **416**, 713 (2002).
[6] Y. Ohno, D. K. Young, B. Beschoten, F. Matsukura, H. Ohno, and D. D. Awschalom, Electrical spin injection in a ferromagnetic semiconductor heterostructure, Nature **402**, 790 (1999).
[7] K. Uchida, S. Takahashi, K. Harii, J. Ieda, W. Koshibae, K. Ando, S. Maekawa, and E. Saitoh, Observation of the spin Seebeck effect, Nature **455**, 778 (2008).
[8] K. Uchida, H. Adachi, T. Ota, H. Nakayama, S. Maekawa, and E. Saitoh, Observation of longitudinal spin-Seebeck effect in magnetic insulators, Appl. Phys. Lett. **97**, 172505 (2010).
[9] S. Mizukami, Y. Ando, and T. Miyazaki, Effect of spin diffusion on Gilbert damping for a very thin permalloy layer in Cu/permalloy/Cu/Pt films, Phys. Rev. B **66**, 104413 (2002).
[10] C. Zucchetti, F. Bottegoni, C. Vergnaud, F. Ciccacci, G. Isella, L. Ghirardini, M. Celebrano, F. Rortais, A. Ferrari, A. Marty, M. Finazzi, and M. Jamet, Imaging spin diffusion in germanim at room temperature, Phys. Rev. B **96**, 014403 (2017).
[11] Y. Tserkovnyak, A. Brataas, and G. E. W. Bauer, Enhanced Gilbert Damping in Thin Ferromagnetic Films, Phys. Rev. Lett. **88**, 117601 (2002).
[12] K. Ando, S. Takahashi, J. Ieda, H. Kurebayashi, T. Trypiniotis, C. H. W. Barnes, S. Maekawa, and E. Saitoh, Electrically tunable spin injector free from the impedance mismatch problem, Nat. Mater. **10**, 655 (2011).
[13] B. Kuerbanjiang, C. Love, D. Kepaptsoglou, Z. Nedelkoski, S. Yamada, A. Ghasemi, Q. M. Ramasse, K. Hamaya, S. A. Cavill, and V. K. Lazarov, Effect of annealing on the structure and magnetic properties of $Co_2FeAl_{0.5}Si_{0.5}$thin films on Ge(111), J. Alloys Compd. **748**, 323 (2018).
[14] M. Yamada, K. Sawano, M. Uematsu, and K. M. Itoh, Suppression of surface segregation of the phosphorous δ-doping layer by insertion of an ultra-thin silicon layer for ultra-shallow ohmic contacts on n-type germanium, Appl. Phys. Lett. **107**, 132101 (2015).
[15] Y. Fujita, M. Yamada, S. Yamada, T. Kanashima, K. Sawano, and K. Hamaya, Temperature-independent spin relaxation in heavily doped *n*-type germanium, Phys. Rev. B **94**, 245302 (2016).
[16] B. Kuerbanjiang, Y. Fujita, M. Yamada, S. Yamada, A. M. Sanchez, P. J. Hasnip, A. Ghasemi, D. Kepaptsoglou, G. Bell, K. Sawano, K. Hamaya, and V. K. Lazarov, Correlation between spin transport signal and heusler/semiconductor interface quality in lateral spin-valve devices, Phys. Rev. B **98**, 115304 (2018).
[17] Y. Fujita, M. Yamada, M. Tsukahara, T. Oka, S. Yamada, T. Kanashima, K. Sawano, and K. Hamaya, Spin Transport and Relaxation up to 250 K in Heavily Doped *n*-Type Ge Detected Using $Co_2FeAl_{0.5}Si_{0.5}$ Electrodes, Phys. Rev. Appl. **8**, 014007 (2017).
[18] M. Yamada, M. Tsukahara, Y. Fujita, T. Naito, S. Yamada, K. Sawano, and K. Hamaya, Room-temperature spin transport in *n*-Ge probed by four-terminal nonlocal measurements, Appl. Phys. Express **10**, 093001 (2017).

[19] L. M. Loong, J. H. Kwon, P. Deorani, C. N. Tung Yu, A. Hirohata, and H. Yang, Investigation of the temperature-dependence of ferromagnetic resonance and spin waves in $Co_2FeAl_{0.5}Si_{0.5}$, Appl. Phys. Lett. **104**, 232409 (2014).

[20] S. Ohya, A. Yamamoto, T. Yamaguchi, R. Ishikawa, R. Akiyama, L. D. Anh, S. Goel, Y. K. Wakabayashi, S. Kuroda, and M. Tanaka, Observation of the inverse spin Hall effect in the topological crystalline insulator SnTe using spin pumping, Phys. Rev. B **96**, 094424 (2017).

[21] M. Koike, E. Shikoh, Y. Ando, T. Shinjo, S. Yamada, K. Hamaya, and M. Shiraishi, Dynamical spin injection into p-type germanium at room temperature, Appl. Phys. Express **6**, 023001 (2013).

[22] A. Jain, et al., Crossover From Spin Accumulation Into Interface States to Spin Injection in the Germanium Conduction Band, Phys. Rev. Lett. **109**, 106603 (2012).

[23] J. C. Rojas-Sánchez, M. Cubukcu, A. Jain, C. Vergnaud, C. Portemont, C. Ducruet, A. Barski, A. Marty, L. Vila, J. P. Attané, E. Augendre, G. Desfonds, S. Gambarelli, H. Jaffrès, J. M. George, and M. Jamet, Spin pumping and inverse spin Hall effect in germanium, Phys. Rev. B **88**, 064403 (2013).

[24] Z. Feng, J. Hu, L. Sun, B. You, D. Wu, J. Du, W. Zhang, A. Hu, Y. Yang, D. M. Tang, B. S. Zhang, and H. F. Ding, Spin Hall angle quantification from spin pumping and microwave photoresistance, Phys. Rev. B **85**, 214423 (2012).

[25] Y. Wang, P. Deorani, X. Qiu, J. H. Kwon, and H. Yang, Determination of intrinsic spin hall angle in Pt, Appl. Phys. Lett. **105**, 152412 (2014).

[26] M. Obstbaum, M. Härtinger, H. G. Bauer, T. Meier, F. Swientek, C. H. Back, and G. Woltersdorf, Inverse spin Hall effect in $Ni_{81}Fe_{19}$/normal-metal bilayers, Phys. Rev. B **89**, 060407(R) (2014).

[27] Y. Zhou, W. Han, L.-T. Chang, F. Xiu, M. Wang, M. Oehme, I. A. Fischer, J. Schulze, R. K. Kawakami, and K. L. Wang, Electrical spin injection and transport in germanium, Phys. Rev. B **84**, 125323 (2011).

[28] S. Oyarzún, A. K. Nandy, F. Rortais, J.-C. Rojas-Sánchez, M.-T. Dau, P. Noël, P. Laczkowski, S. Pouget, H. Okuno, L. Vila, C. Vergnaud, C. Beigné, A. Marty, J.-P. Attané, S. Gambarelli, J.-M. George, H. Jaffrès, S. Blügel, and M. Jamet, Evidence for spin-to-charge conversion by Rashba coupling in metallic states at the Fe/Ge(111) interface, Nat. Commun. **7**, 13857 (2016).

[29] S. Ohya, D. Araki, L. D. Anh, S. Kaneta, M. Seki, H. Tabata, and M. Tanaka, Efficient intrinsic spin-to-charge current conversion in an all-epitaxial single-crystal perovskite-oxide heterostructure of $La_{0.67}Sr0.33MnO_3$/$LaAlO_3$/$SrTiO_3$, Phys. Rev. Res. **2**, 012014(R) (2020).